Photogeneration of Reactive Transient Species Upon Irradiation of Natural Water Samples: Formation Quantum Yields in Different Spectral Intervals, and Implications for the Photochemistry of Surface Waters.

Photogeneration of reactive transient species upon irradiation of natural water samples: Formation quantum yields in different spectral intervals, and implications for the photochemistry of surface waters

Andrea Marchisio,[a] Marco Minella,[a] Valter Maurino,[a] Claudio Minero,[a] Davide Vione[a,b]*

[a] *Università di Torino, Dipartimento di Chimica, Via Pietro Giuria 5, 10125 Torino, Italy.*
[b] *Universita' di Torino, Centro Interdipartimentale NatRisk, Via L. Da Vinci 44, 10095 Grugliasco (TO), Italy.*

* Corresponding author. Fax +39-011-6705242. E-mail: *davide.vione@unito.it*

Abstract

Chromophoric dissolved organic matter (CDOM) in surface waters is a photochemical source of several transient species such as CDOM triplet states (^{3}CDOM*), singlet oxygen ($^1O_2$) and the hydroxyl radical ($^\bullet$OH). By irradiation of lake water samples, it is shown here that the quantum yields for the formation of these transients by CDOM vary depending on the irradiation wavelength range, in the order UVB > UVA > blue. A possible explanation is that radiation at longer wavelengths is preferentially absorbed by the larger CDOM fractions, which show lesser photoactivity compared to smaller CDOM moieties. The quantum yield variations in different spectral ranges were definitely more marked for ^{3}CDOM* and $^\bullet$OH compared to $^1O_2$. The decrease of the quantum yields with increasing wavelength has important implications for the photochemistry of surface waters, because long-wavelength radiation penetrates deeper in water columns compared to short-wavelength radiation. The average steady-state concentrations of the transients (^{3}CDOM*, $^1O_2$ and $^\bullet$OH) were modelled in water columns of different depths, based on the experimentally determined wavelength trends of the formation quantum yields. Important differences were found between such modelling results and those obtained in a wavelength-independent quantum yield scenario.

Keywords: Indirect Photochemistry; Photogeneration Quantum Yields; Environmental Photochemistry; Sensitised Photolysis; Spectral Intervals.

Introduction

Chromophoric dissolved organic matter (CDOM) is the main sunlight absorber in surface waters up to at least 500 nm (Loiselle et al., 2009; Bracchini et al., 2011). By absorbing sunlight, CDOM attenuates the penetration of UV and most notably UVB radiation in water columns and protects living organisms from the associated harmful effects (Rose et al., 2009; Ruiz-Gonzales et al., 2013). Radiation absorption by CDOM causes several modifications in the absorbing material, the most evident one being its photobleaching (loss of absorbance due to the transformation of chromophoric groups into non-chromophores) (Sulzberger and Durisch-Kaiser, 2009; Zhang et al., 2013). Some degree of photomineralisation has also been observed, most notably under acidic conditions (Anesio and Graneli, 2003, 2004; Vione et al., 2009). However, the most effective pathway leading to CDOM mineralisation is probably a combination of photochemical and microbial processes (Vahatalo and Wetzel, 2008), where irradiation enhances the bioavailability of the organic material (Vahatalo et al., 2003; Piccini et al., 2013).

Another important consequence of radiation absorption by CDOM is the generation of reactive transient species that are involved into the transformation of (C)DOM itself and of xenobiotics. In the latter case one speaks of indirect photolysis of pollutants (Canonica et al., 2006; Vione et al., 2014). The photogenerated transients are CDOM triplet states (^{3}CDOM*), singlet oxygen ($^1O_2$), the hydroxyl radical ($^\bullet$OH), superoxide ($O_2^{-\bullet}$) and other still poorly characterised radical species arising from the photooxidation of organic matter (*e.g.* peroxy radicals, ROO$^\bullet$) (Hoigné, 1990; Canonica and Freiburghaus, 2001; Grebel et al., 2011). Of the above transients, ^{3}CDOM*, $^1O_2$ and $^\bullet$OH are well known to take part to the degradation of various biorefractory xenobiotics, including emerging pollutants (Boreen et al., 2003; Ruggeri et al., 2013), but secondary pollutants can also be formed in the relevant processes (Iesce et al., 2004 ; Méndez-Díaz et al., 2014). The production of $^1O_2$ directly stems from that of ^{3}CDOM* (reactions 1,2, where ISC = Inter-System Crossing) (Hoigné, 1990), while the pathways leading to $^\bullet$OH from irradiated CDOM are more controversial. Reactions (3-8) show possible H_2O_2-associated processes, where Fe^{III}-L is an organic ferric complex (a CDOM component as well; Xiao et al., 2013) and R is an easily oxidised organic compound. However, it is well known that part of the $^\bullet$OH production by CDOM does not depend on H_2O_2 (Page et al., 2011). In this case, possible pathways are either the fragmentation of oxygen-containing radical species or the oxidation of H_2O/OH^- by photoexcited CDOM. Some evidence of the latter pathway has been obtained with some triplet sensitisers as CDOM proxies (Sur et al., 2011), but the significance of these results for CDOM photochemistry is still highly uncertain.

$$\text{CDOM} + h\nu \rightarrow {}^1\text{CDOM}^* \xrightarrow{ISC} {}^3\text{CDOM}^* \quad (1)$$

$$^3\text{CDOM}^* + O_2 \rightarrow \text{CDOM} + {}^1O_2 \quad (2)$$

$^3CDOM^* + R \rightarrow CDOM^{-\bullet} + R^{+\bullet}$ (3)

$CDOM^{-\bullet} + O_2 \rightarrow CDOM + O_2^{-\bullet}$ (4)

$2\ O_2^{-\bullet} + 2\ H^+ \rightarrow H_2O_2 + O_2$ (5)

$Fe^{III}\text{-}L + h\nu \rightarrow Fe^{2+} + L^{+\bullet}$ (6)

$H_2O_2 + h\nu \rightarrow 2\ ^\bullet OH$ (7)

$Fe^{2+} + H_2O_2 \rightarrow FeOH^{2+} + {}^\bullet OH$ (8)

CDOM is the only source of ^{3}CDOM* and $^1O_2$ and it is an important $^\bullet$OH source as well (Glover and Rosario-Ortiz, 2013; Lee et al., 2013). Significant CDOM absorption would still take place in deep waters, where the sunlight spectrum is depleted of UV radiation (which is absorbed in the upper water layers) (Loiselle et al., 2008). Some processes induced by irradiated CDOM (*e.g.* the reaction of pollutants with ^{3}CDOM* and $^1O_2$) are potentially more important in deep water bodies (De Laurentiis et al., 2013a), where the ability of CDOM photochemistry to be triggered by visible radiation is a major factor. In this context, the efficiency (quantum yield) by which irradiated CDOM produces different reactive transients as a function of the absorbed wavelength(s) has major importance.

Quantum yields of transient production by humic substances (HS) under UVC radiation have been determined in order to assess indirect photoreactions in UV water treatment. Comparison with results obtained under real or simulated sunlight suggests that HS quantum yields vary depending on the spectral range (Lester et al., 2013). It is also well known that the quantum yield of $^\bullet$OH photogeneration in natural waters is higher in the UVB than in the UVA region (Mopper and Zhou, 1990; Sharpless and Blough, 2014), and variations with wavelength have been reported for the quantum yield of $^1O_2$ generation by humic and fulvic substances (Sharpless, 2012). Unfortunately, very little is known about the wavelength trend under sunlight-relevant conditions of the formation quantum yields of ^{3}CDOM* (Sharpless and Blough, 2014), from which $^1O_2$ is directly formed and $^\bullet$OH might also arise (at least indirectly, see reactions 3-5,8). Moreover, few or no data are available on the photochemical generation of the main transients (^{3}CDOM* and $^1O_2$, in addition to $^\bullet$OH) upon irradiation of natural water samples (as opposed to CDOM isolates) in wavelength intervals of environmental significance. This is a knowledge gap when modelling photochemistry in whole columns of natural water bodies.

This paper undertakes the task of filling this gap, by measuring the formation quantum yields of ^{3}CDOM*, $^1O_2$ and $^\bullet$OH in different spectral intervals, in natural water samples taken from lakes that differ for trophic state and surrounding environment. The significance of the results for the modelling of the photochemistry of surface waters is assessed as well.

Experimental

Reagents and materials. $NaNO_3$ (purity grade 99%), $MgSO_4$ (99%), $CaCl_2 \cdot 2\ H_2O$ (98%), NH_4Cl (99.5%), HCl (37%), K_2CO_3 (99%), $NaHCO_3$ (99.5%), 2,4,6-trimethylphenol (97%), furfuryl alcohol (98%), phenol (99%), 2,4-dinitrophenylhydrazine (97%), methanol (gradient grade), tetrabutylammonium hydroxide (98%) and 2-nitrobenzaldehyde (98%) were purchased from Aldrich, $NaNO_2$ (97%) and H_3PO_4 (85%) from Carlo Erba, KNO_3 (99%), KCl (99%), benzene (SupraSolv) and CCl_4 (SupraSolv) from Merck/VWR Int., NaCl (99.5%) and methanesulphonic acid (98%) from Fluka, acetonitrile (gradient grade) from Scharlau.

Lake water sampling and characterisation. Water was sampled from the epilimnion at centre lake (reached by boat, with the exception of the small Lake Balma) in summer 2013. Lake details are given in Table S1 of the Supplementary Material (hereafter SM). With one exception, the study lakes were characterised by relatively high amounts of dissolved organic matter. The rationale for this choice was the need to obtain measurable formation of reactive transients upon irradiation of the samples at longer wavelengths. After sampling, the lake water was transported to the laboratory under refrigeration, vacuum filtered (0.22 μm filter membranes, Millipore) soon upon arrival and refrigerated (4 °C) till further processing.

Inorganic ions were determined by ion chromatography, with the exception of nitrite that underwent pre-column derivatisation with 2,4-dinitrophenylhydrazine followed by analysis by reverse-phase high-performance liquid chromatography with diode array detection (HPLC-DAD) (Kieber and Seaton, 1995). The dissolved organic carbon (DOC), inorganic carbon (IC) and total nitrogen (TN) of the samples was measured with a Shimadzu TOC-VCSH instrument. Organic matter was characterised by UV-Vis absorption spectroscopy and by fluorescence Excitation-Emission Matrix (EEM) (Coble, 1996). Important spectral parameters thus obtained were the spectral slope *S* and the spectral index E_2/E_3 (absorbance ratio, A_{250nm}/A_{365nm}). Analytical details of the mentioned techniques and other details of lake water characterisation are reported in the SM.

Irradiation experiments. The formation of reactive transients was measured by addition of probe molecules (Al Housari et al., 2010). Lake water samples (20 mL) were spiked with trimethylphenol (TMP, ^{3}CDOM* probe, 1 mM initial concentration), furfuryl alcohol (FFA, $^1O_2$ probe, 0.1 mM) or benzene ($^{\bullet}$OH probe, 2 mM) and placed in cylindrical Pyrex glass cells (4.0 cm diameter, 2.3 cm height, with a lateral neck tightly closed with a screw cap). The cells were then placed under the chosen radiation source, irradiated for up to 30 h and magnetically stirred during irradiation. A pictorial scheme of the irradiation set-up is provided in the SM (Figure S1). Three different lamps were used: Philips TL 01 (20W) with emission maximum at 313 nm (UVB), Philips TLK 05 (40 W) with emission

maximum at 365 nm (UVA), and a blue lamp Philips TLK 03 (40 W) with emission maximum at 420 nm. The UVB lamp has secondary emission bands in the UVA and visible, but the decrease of lake water absorbance with increasing wavelength limits the absorption outside the UVB range. The lamp emission spectra (spectral photon flux density $p°(\lambda)$ as a function of wavelength, units of Einstein L^{-1} s^{-1} nm^{-1}) were obtained by combining spectrophotometric measures and chemical actinometry with 2-nitrobenzaldehyde (Galbavy et al., 2010; see SM for the detailed procedure). Lamp spectra are reported in Figure 1, together with the absorption spectra of the studied lake water samples ($A_1(\lambda)$, largely accounted for by CDOM absorption in the considered wavelength range). See SM for the determination of $A_1(\lambda)$. The temperature of the irradiated solutions was 30±2 °C.

In preliminary experiments, lake water was irradiated with a 150 W LOT-Oriel Xe arc lamp equipped with 10-40 nm bandwidth filters (full width at half maximum), to carry out narrow-band irradiation. Unfortunately, the filtered radiation was not intense enough to cause significant transformation of the probe molecules within reasonable irradiation times, not even by considerably decreasing the initial concentrations of the TMP and FFA probes to better appreciate their transformation. For this reason, the choice of the irradiation devices was shifted toward the already described Philips lamps, where the lower spectral resolution was compensated for by higher irradiance.

The solutions in the cells were irradiated from the top and the optical path length was 1.6 cm. After the scheduled irradiation time, 1 mL aliquots were withdrawn from the cells and analysed by HPLC-DAD to monitor the time evolution of TMP, FFA or phenol (formed from benzene upon reaction with $^{\bullet}OH$). Analytical conditions are reported in the SM.

Control experiments were carried out. To assess the photogeneration of $^{\bullet}OH$ by nitrate and nitrite in the irradiated samples, solutions in Milli-Q water containing 2 mM benzene and the same nitrate or nitrite levels as determined in lake water were irradiated under the UVB, UVA and blue lamps. The time evolution of phenol was then monitored as described above. To assess the importance of processes such as direct photolysis or hydrolysis of the probe molecules and the possible residual biological activity of the lake water (decreased but possibly not totally eliminated by filtration), the following control experiments were executed: *(i)* irradiation of solutions of TMP, FFA and benzene in Milli-Q water (natural pH around 7, not far from that of lake water), and *(ii)* monitoring of the behaviour of the probe molecules in lake water in the dark. In the latter case, to ensure comparable temperature and stirring conditions with the irradiation experiments, cells were wrapped in double aluminium foil and placed under the same lamps used for irradiation. No transformation was observed in lake water in the dark, while the (usually limited) transformation in Milli-Q water under irradiation was taken into account in calculations (*vide infra*). All the irradiation and control experiments were carried out in duplicate.

Kinetic data treatment and assessment of transient formation. TMP (^{3}CDOM* probe, 1 mM initial concentration) was added in excess to the lake water so that it could be the main sink for ^{3}CDOM*. The rationale was to use an elevated TMP concentration (still allowing an easy assessment of its degradation), to minimise the impact of uncertainties associated with the reaction rate constant between TMP and ^{3}CDOM* and with the quenching rate constant of ^{3}CDOM* (*vide infra*) (Halladja et al., 2007; Al Housari et al., 2010; Golanoski et al., 2012). Uncertainties are understandably important given the poorly known nature of CDOM, and of ^{3}CDOM* as a consequence. The elevated probe concentration also ensures that TMP prevalently reacts with short-lived triplet states, minimising the possible contribution of longer-lived species that are also produced by CDOM irradiation (Canonica and Freiburghaus, 2001).

The degradation of TMP in the studied systems followed zero-order kinetics and its time trend could be fit with $[TMP]_t = [TMP]_o - k_{TMP}\, t$, where $[TMP]_o = 10^{-3}$ M, thereby obtaining k_{TMP} (s^{-1} units) by data fit. The error on k_{TMP} was derived as the fit uncertainty on the average of replicate runs. The initial transformation rate (in M s^{-1} units) is $R_{TMP} = k_{TMP}\,[TMP]_o$. The reaction between TMP and ^{3}CDOM*, with second-order rate constant $k_{TMP,^3CDOM*} \sim (2\text{-}3)\cdot 10^9$ M^{-1} s^{-1} (determined upon UV irradiation of either humic substances or surface-water CDOM; Halladja et al., 2007; Al Housari et al., 2010), is in competition with the quenching of ^{3}CDOM* by reaction with O_2 and internal conversion. The quenching process can be described by a pseudo-first order rate constant $k' \sim 5\cdot 10^5$ s^{-1} (Canonica and Freiburghaus, 2001). One obtains:

$$R_{TMP} = R_{^3CDOM*} \frac{k_{TMP,^3CDOM*}[TMP]_o}{k_{TMP,^3CDOM*}[TMP]_o + k'} + R_{TMP}^{Milli-Q} \qquad (9)$$

where $R_{^3CDOM*}$ is the formation rate of ^{3}CDOM* and $R_{TMP}^{Milli-Q}$ is the transformation rate of TMP in Milli-Q water (limited but not negligible). Both rates are in M s^{-1} units. $R_{TMP}^{Milli-Q}$ might possibly be accounted for, at least in part, by direct photolysis, although TMP has very low absorption above 300 nm (actually, TMP did not interfere with absorption by lake water). However, the absorbance of lake water above 300 nm was sufficiently low (0.1 or lower) that it was not necessary to correct $R_{TMP}^{Milli-Q}$ for the radiation screening by lake *vs.* Milli-Q water (the correction would be considerably lower than the experimental error on R_{TMP}). Moreover, $[TMP]_o$ = 1 mM ensures that $k_{TMP,^3CDOM*}[TMP]_o$ would be considerably higher than k', which limits the impact of the uncertainties on the values of k' (assumed to be equal to $5\cdot 10^5$ s^{-1}). At elevated $[TMP]_o$ it would be $R_{TMP} \approx R_{^3CDOM*} + R_{TMP}^{Milli-Q}$ and, consequently, also the uncertainty on $k_{TMP,^3CDOM*}$ (assumed to be equal to $2.5\cdot 10^9$ M^{-1} s^{-1}) would have limited influence on R_{TMP}. The value of $R_{^3CDOM*}$ was obtained from equation (9), because R_{TMP} and $R_{TMP}^{Milli-Q}$ were measured and all the other quantities are known.

FFA ($^1O_2$ probe, 0.1 mM initial concentration) underwent the most marked transformation under the UVB lamp (up to 30% of the initial concentration), and its time trend could be approximated quite well with a zero-order kinetics. By assuming that $^1O_2$ either reacts with FFA (with second-order rate constant $k_{FFA,^1O_2}$ = $1.2 \cdot 10^8$ M^{-1} s^{-1}; Wilkinson and Brummer, 1981) or undergoes inactivation by collision with the solvent (with pseudo-first order rate constant k" = $2.5 \cdot 10^5$ s^{-1}; Rodgers and Snowden, 1982), one gets the initial transformation rate R_{FFA} as follows:

$$R_{FFA} = R_{^1O_2} \frac{k_{FFA,^1O_2}[FFA]_o}{k_{FFA,^1O_2}[FFA]_o + k''} + R_{FFA}^{Milli-Q} \quad (10)$$

where $R_{^1O_2}$ is the formation rate of $^1O_2$, $[FFA]_o$ (10^{-4} M) the initial concentration of FFA and $R_{FFA}^{Milli-Q}$ the degradation rate of FFA in Milli-Q water. All rates are in M s^{-1} units. Similarly to the case of TMP, it was not necessary to correct $R_{FFA}^{Milli-Q}$ for the light screening of lake water. $R_{^1O_2}$ was obtained from equation (10).

The time trend of the formation of phenol (P) from benzene (B, initial concentration 2 mM) could be fitted quite well with the equation $[P]_t = k_P^f [B]_o (k_P^d - k_B^d)^{-1} (e^{-k_B^d t} - e^{-k_P^d t})$ (De Laurentiis et al., 2013b), where $[P]_t$ is the concentration of phenol at the time *t*, $[B]_o$ is the initial concentration of benzene, k_P^f is the first-order formation rate constant of phenol from benzene, and k_P^d and k_B^d are the first-order degradation rate constants of phenol and benzene, respectively. Concentrations are in molar units, while the rate constants have units of s^{-1}. The initial formation rate of phenol (M s^{-1} units) can be obtained as the initial slope ($R_P = k_P^f [B]_o$). The photogenerated $^\bullet OH$ can react either with benzene, or with the natural $^\bullet OH$ scavengers present in the water samples. The first-order natural scavenging rate constant of $^\bullet OH$ by lake water is in the order of 10^5 s^{-1} (Vione et al., 2014), to be compared with the first-order scavenging rate constant of $^\bullet OH$ by benzene, $k_B = k_{B,^\bullet OH}[B]_o$. Considering that $k_{B,^\bullet OH}$ = $7.8 \cdot 10^9$ M^{-1} s^{-1} (second-order reaction rate constant between benzene and $^\bullet OH$; Buxton et al., 1988) and $[B]_o = 2 \cdot 10^{-3}$ M, k_B (s^{-1} units) would be around two orders of magnitude higher than the natural $^\bullet OH$ scavenging rate constant. Therefore, one can assume that benzene reacts with the totality of photoproduced $^\bullet OH$. By assuming a 95% yield of phenol from benzene + $^\bullet OH$ (Deister et al., 1990), one gets:

$$R_P = 0.95\, R_{^\bullet OH}^{CDOM} + R_P^{NO_3^-} + R_P^{NO_2^-} + R_P^{Milli-Q} \quad (11)$$

All the rates in equation (11) have M s^{-1} units. $R_{^\bullet OH}^{CDOM}$ is the formation rate of $^\bullet OH$ by CDOM and $R_P^{Milli-Q}$ is the initial formation rate of phenol upon irradiation of 2 mM benzene in Milli-Q water. $R_P^{NO_3^-}$ and $R_P^{NO_2^-}$ are the initial formation rates of phenol due to $^\bullet OH$, photogenerated by nitrate and nitrite ions

occurring in lake water (De Laurentiis et al., 2013b). The latter were measured upon irradiation of 2 mM benzene in the presence of nitrate and nitrite in Milli-Q water, at the same concentration levels as those detected in lake water. For reasons already discussed and because of the low values of $R_P^{NO_3^-}$, $R_P^{NO_2^-}$ and $R_P^{Milli-Q}$, it was not necessary to introduce corrections for the absorption of radiation in lake *vs.* Milli-Q water. Actually, R_P was in the 10^{-12}-10^{-11} M s^{-1} range, $R_P^{NO_2^-}$ in the 10^{-14} M s^{-1} one, $R_P^{NO_3^-}$ around 10^{-13} M s^{-1}, and $R_P^{Milli-Q}$ around 10^{-14} M s^{-1}. Moreover, $R_P^{NO_2^-}$ and $R_P^{NO_3^-}$ were negligible under blue-lamp irradiation.

If one knows the formation rate R_i of the transient species *i* (^{3}CDOM*, $^1O_2$ or $^\bullet$OH) in the irradiated sample, the formation quantum yield can be calculated as $\Phi_i = R_i (P_a)^{-1}$. P_a (units of Einstein L^{-1} s^{-1}) is the photon flux absorbed by the natural water sample (mostly accounted for by CDOM; Loiselle et al., 2009), which can be expressed as follows (Braslavsky, 2007):

$$P_a = \int_\lambda p°(\lambda)[1-10^{-A_1(\lambda)b}]d\lambda \qquad (12)$$

where $p°(\lambda)$ (units of Einstein L^{-1} s^{-1} nm^{-1}) is the incident spectral photon flux density, $A_1(\lambda)$ (units of cm^{-1}) is the absorbance of the water sample over an optical path length of 1 cm, and b = 1.6 cm is the optical path length in solution.

Measurement biases are theoretically possible. TMP could react with ^{3}CDOM*, $^1O_2$ and $^\bullet$OH (Al Housari et al., 2010), but $R_{\bullet OH}$ was 2-3 orders of magnitude lower than R_{TMP} and the possible reaction between TMP and $^\bullet$OH would not affect significantly the determination of $R_{^3CDOM^*}$. Moreover, considering that $^1O_2$ is produced by ^{3}CDOM* in reaction (2) and given the $^1O_2$ reaction rate constant with TMP, $^1O_2$ is unlikely to account for more than 4% of TMP transformation (De Laurentiis et al., 2013b). For similar reasons as above, $^\bullet$OH would not account for a significant fraction of FFA transformation (from the values of $R_{\bullet OH}^{CDOM}$ and R_{FFA} one obtains that the expected bias is below 5%).

In contrast, ^{3}CDOM* could interfere with the measurement of $R_{^1O_2}$ (Al Housari et al., 2010). The addition of $^1O_2$ scavengers such as NaN_3 to check for such an effect may be poorly conclusive, because triplet states have been shown to undergo fast reaction with N_3^- and with other compounds used as $^1O_2$ scavengers (Maddigapu et al., 2010). The possible reaction between ^{3}CDOM* and FFA could introduce a bias in R_{FFA} (which will be taken into account when discussing the $\Phi_{^1O_2}$ results), but it would not be able to affect significantly the formation of $^1O_2$ through triplet-state quenching. The CDOM triplet states are often more reactive than $^1O_2$ but, considering that FFA as $^1O_2$ probe is particularly reactive toward singlet oxygen, one could assume comparable reactivity of FFA with $^1O_2$ and ^{3}CDOM*. Given the typical kinetics of ^{3}CDOM* decay (*k'*), one gets that 0.1 mM FFA could scavenge ~2% of the photogenerated ^{3}CDOM*.

Finally, hydroxylation of $^{\bullet}$OH probe molecules could also occur in the absence of free $^{\bullet}$OH, upon irradiation of CDOM that could produce the so-called "low-level" hydroxylating species. This issue could bias the determination of $R_{^{\bullet}OH}^{CDOM}$. However, such an effect depends on the type of CDOM and it is often not observed. When operational, it is usually important for DOC values above 10 mg C L^{-1}, which is higher than the DOC levels of the studied lake water samples (Page et al., 2011).

Results and Discussion

Characterisation of lake water

The results of the chemical and spectroscopic characterisation of the studied lake water samples are summarised in Table 1. With the exception of Sottano della Sella (SdS), the samples contained over 3 mg C L^{-1} DOC. Moreover, the low concentration values of nitrate and nitrite made it easier to assess the photochemical production of $^{\bullet}$OH by CDOM. Interestingly, the two mountain lakes (Balma and SdS) had lower inorganic carbon levels and pH values compared to the lowland lakes (see Table 1). While pH might affect lake-water photochemistry, much larger differences than those observed in the studied samples would be required for pH to be really an issue (Vione et al., 2009). Actually, a much more important effect on CDOM and its properties could be provided by the fact that the mountain lakes are above the tree-line and surrounded by alpine meadows and exposed rocks, while the other lakes are located in partially forested areas (De Laurentiis et al., 2012).

As far as the spectroscopic parameters are concerned, one can see that water from the mountain lakes (Balma and SdS) had lower values of E_2/E_3 and S compared to the lowland lakes. In the two mountain lakes the absorption spectra underwent a less steep decrease with increasing wavelength, which could be accounted for by an elevated molecular weight and/or aromaticity of CDOM (Peuravuori and Pihlaja, 1997). Indeed, molecules with several conjugated double bonds and/or aromatic rings (or large aggregates with important inter-molecular interactions) have absorption bands that tend to be shifted towards the visible. In the case of large aggregates, however, the more efficient absorption of sunlight is offset by the fact that molecular interactions (and particularly charge-transfer processes) tend to favour the internal conversion that inhibits both photophysical (*e.g.* fluorescence emission) and photochemical processes (Del Vecchio and Blough, 2004).

The fluorescence EEM spectra of the water samples are reported in the SM (Figure S2). They show the typical signatures of the components of surface-water CDOM, namely proteins and humic/fulvic substances (Coble, 1996). Humic components were particularly intense in Avigliana, Candia and Balma, while protein signals were prominent in Viverone. Fluorescence was very low in SdS, possibly because of the low DOC content. The higher signal of proteins compared to humic substances (HS),

observed in SdS, is typical of many oligotrophic lakes located above the tree-line (De Laurentiis et al., 2012).

Quantum yields of transient formation

The experimental time trends of TMP, FFA and phenol in lake and Milli-Q water under the UVB, UVA and blue lamps are reported in the SM, Figures S3-S5. Table 2 reports the initial rates of: TMP and FFA transformation (measured), phenol formation (measured), and ^{3}CDOM*, $^1O_2$ and $^\bullet$OH formation (calculated) for the studied lake water samples under the different irradiation conditions. Figure 2 reports the measured quantum yields for the formation of ^{3}CDOM* (2a), $^1O_2$ (2b) and $^\bullet$OH (2c) in the three spectral intervals.

The ^{3}CDOM* quantum yields ($\Phi_{^3CDOM^*}$) significantly decreased with increasing wavelength (compare differences in quantum yields with the associated error bands), from values of 0.02-0.06 in the UVB to < 0.01 in the blue. The quantum yield decrease, evident for all the lake water samples, was particularly marked for SdS that had the highest UVB $\Phi_{^3CDOM^*}$ and the lowest blue $\Phi_{^3CDOM^*}$. The low spectral slope of SdS might be consistent with a significant occurrence of charge-transfer bands from large aggregates, which would absorb radiation at elevated wavelengths. In this scenario, the absorption of blue light by SdS might be associated with efficient processes of internal conversion, which would cause non-radiative and non-reactive deactivation of the excited states and would considerably decrease the relevant $\Phi_{^3CDOM^*}$ values (Sharpless and Blough, 2014; Mostafa et al., 2014). A similar phenomenon, albeit less marked, might be operational in the other samples and it would account for the wavelength decrease of $\Phi_{^3CDOM^*}$. Indeed, because of internal conversion phenomena, high-molecular weight CDOM (HMW CDOM) is photochemically less reactive than the low-molecular weight one (LMW CDOM) (Cavani et al., 2009; Trubetskoj et al., 2009; Mostafa and Rosario-Ortiz, 2013; Mostafa et al., 2014), but it absorbs a larger fraction of visible radiation.

It is unfortunately not easy to compare the wavelength-dependent values of $\Phi_{^3CDOM^*}$ obtained here with those measured in previous papers that made use of real or simulated sunlight, but comparison with previous works that used UVA radiation is possible. The UVA-$\Phi_{^3CDOM^*}$ data reported here are quite in the range of those obtained by irradiation of samples from lakes located in temperate regions (De Laurentiis et al., 2012). Interestingly, they are much lower than those reported for lakes in Antarctica (De Laurentiis et al., 2013b), but in that case it is possible that the unusually elevated reactivity was closely linked with extreme environmental features (*e.g.* extensive ice cover protecting CDOM from photodegradation/photobleaching). Coherently with the wavelength trend of $\Phi_{^3CDOM^*}$ obtained here, the quantum yield of TMP disappearance with humic substance isolates was higher under UVC than upon irradiation at $\lambda > 300$ nm (Lester et al., 2013).

The trend of $\Phi_{^1O_2}$ in the different spectral intervals is reported in Figure 2b. In the case of lake SdS, the quantum yield of $^1O_2$ formation under blue light could not be measured: the rate of FFA transformation was not different from that observed in Milli-Q water. In the case of the lowland lakes (Avigliana, Candia and partially Viverone) the decrease of $\Phi_{^1O_2}$ with increasing wavelength was rather limited, and certainly much less marked compared to the wavelength trend of $\Phi_{^3CDOM^*}$. In contrast, the $\Phi_{^1O_2}$ wavelength trend was more marked for the mountain lakes (Balma and SdS). A ^{3}CDOM* bias on the assessment of R_{FFA} and $\Phi_{^1O_2}$ cannot be excluded, but the bias should be highest for UVB and lowest for blue irradiation as suggested by the $\Phi_{^3CDOM^*}$ trend. Indeed, a ^{3}CDOM*-dominated degradation of FFA should produce a wavelength trend of $\Phi_{^1O_2}$ that is similar to that of $\Phi_{^3CDOM^*}$. This issue and the associated bias cannot be excluded for Balma and SdS, but it is clearly not the case for the lowland lakes. A moderate decrease of $\Phi_{^1O_2}$ with increasing wavelength (very similar to the $\Phi_{^1O_2}$ trend for the three lowland lakes) has already been reported by Sharpless (2012) upon irradiation of humic substances, although the $\Phi_{^1O_2}$ values of humic material were about twice those reported here for lake water. By excluding a variation with wavelength of the triplet decay kinetics, Sharpless (2012) supposed that the $\Phi_{^1O_2}$ wavelength trend might possibly follow that of $\Phi_{^3CDOM^*}$. The findings of the present work suggest that this may not be exactly the case and that there would be some enhancement of $^1O_2$ production efficiency from ^{3}CDOM* at longer wavelengths. Variable kinetics of triplet decay could account for the experimental data if one assumes that internal conversion phenomena were slower under blue light, where absorption by HMW CDOM should prevail. This assumption looks unjustified, however, because it is highly at variance with the current understanding of HMW CDOM photophysics and photochemistry (Sharpless and Blough, 2014).

Two possible explanations could be advanced for the observed phenomenon. First of all, the large molecules and inter-molecular aggregates have hydrophobic cores where $^1O_2$ reaches an elevated steady-state concentration (Latch and McNeill, 2006). Considering that the photoactivity of HMW CDOM would be kept low by internal conversion, the elevated levels of singlet oxygen in hydrophobic cores could be accounted for by longer $^1O_2$ lifetimes than in solution (Minella et al., 2013). If this is the case, it might be possible for $^1O_2$ to diffuse from CDOM cores into the solution bulk. This phenomenon cannot be highlighted by irradiation at shorter wavelengths (Minella et al., 2013), where smaller molecules (LMW CDOM) would account for most of the $^1O_2$ photoproduction (Mostafa and Rosario-Ortiz, 2013). In contrast, under longer-wavelength irradiation, the photochemistry of LMW CDOM would be scarcely operational and the effects of HMW CDOM may become evident. In this scenario, at the longer wavelengths, the degradation of FFA would measure both the bulk $^1O_2$ and that escaping from the hydrophobic cores of HMW CDOM. In some cases one might even observe $\Phi_{^1O_2} > \Phi_{^3CDOM^*}$ at longer wavelengths because of the additional $^1O_2$ source (in contrast, from a simple kinetic model based on ^{3}CDOM* formation and reactivity in the solution bulk, one would expect $\Phi_{^1O_2} \leq \Phi_{^3CDOM^*}$).

Note that, while FFA is likely to only react with solution-bulk $^1O_2$ (whichever its origin), TMP could undergo some partitioning into the hydrophobic cores where it could react with the triplet states there formed. However, this process is unlikely to be important for two reasons: *(i)* hydrophobic cores are more common in HMW CDOM and particles, but these species have been shown to play a negligible role in TMP transformation under UV irradiation (Minella et al., 2013); *(ii)* TMP degradation in hydrophobic compartments would be highlighted under blue/visible irradiation, where the photochemistry of HMW CDOM prevails. However, they are exactly the conditions where one observes, in contrast, a relative increase in the efficiency of FFA degradation compared to TMP. If TMP mainly reacts with ^{3}CDOM* in the solution bulk, the results are more easily explained: differently from $^1O_2$, the triplet states of HMW CDOM would not be able to diffuse into the bulk aqueous phase.

An alternative explanation to the hydrophobic core hypothesis is that irradiation under blue light only yields triplet states with low energy. In this case, formation of high-energy (and presumably more reactive) triplets could be prevented by the insufficient energy of the incoming photons. Low-energy triplet states might still be able to transfer energy to O_2 to produce $^1O_2$, but they might be unable to trigger the transformation of TMP. One would thus explain why $\Phi_{^3CDOM^*}$ (determined from the R_{TMP} data) decreased to a higher extent than $\Phi_{^1O_2}$ when increasing the irradiation wavelength. In this scenario, the use of TMP as ^{3}CDOM* probe under blue irradiation would induce an underestimation of ^{3}CDOM* formation. The $\Phi_{^3CDOM^*}$ data thus obtained would nevertheless be relevant to surface-water photochemistry, because triplet states that are unable to induce TMP degradation are also unlikely to trigger significant transformation of organic pollutants, most of which are less electron-rich than TMP.

Figure 2c reports the values of $\Phi_{^\bullet OH}^{CDOM}$ for the studied lakes in the different spectral intervals. The decrease of the quantum yield with increasing wavelength is consistent with previous reports (Mopper and Zhou, 1990). The only partial exception is represented by Viverone, because the formation of phenol under blue-light irradiation was unexpectedly a bit higher compared to the case of UVA (see SM, Figure S5), despite lower absorption by lake water in the blue as shown in Figure 1. Interestingly, this unusual photochemical behaviour was not combined with peculiar features of either chemical composition or spectroscopic properties (see Table 1).

Within the same lake, there was a significant correlation between the values of $\Phi_{^\bullet OH}^{CDOM}$ and $\Phi_{^3CDOM^*}$ in each studied spectral interval ($R^2 > 0.98$, see Table S2 in SM). The only exception was Viverone, where $R^2 = 0.60$, mostly because of the anomalous wavelength trend of $\Phi_{^\bullet OH}^{CDOM}$ mentioned above. One might hypothesise that Viverone water contains a small amount of chromophores, accounting for a limited fraction of the UV absorbance but having absorption extended in the blue region, that show elevated efficiency towards $^\bullet$OH photoproduction. In the other cases, the correlation may be consistent with an involvement of ^{3}CDOM* in the photochemical generation of $^\bullet$OH. Apart from the controversial possibility that ^{3}CDOM* may directly oxidise OH^- and possibly H_2O, the triplet

states could be indirectly involved in $^{\bullet}OH$ generation through photo-Fenton or similar reactions (see reactions 3-8). Note, however, that the content of dissolved Fe in the filtered lake water samples was very low (< 2.5 μg L^{-1} levels, see Table 1).

The significance of comparisons with other studies is lowered by differences in irradiation wavelength ranges. However, the $\Phi_{^{\bullet}OH}^{CDOM}$ values found here are not far from those reported for natural water samples and their constituents (White et al., 2003; Sharpless and Blough, 2014) or for bulk effluent organic matter, EfOM (Lee et al., 2013; interestingly, there appears to be better agreement with the non-humic EfOM fractions). The values reported in Figure 2c are about an order of magnitude lower than those observed upon irradiation of lake water samples from Antarctica (De Laurentiis et al., 2013b), the unusual photoactivity of which has already been discussed.

When comparing the formation quantum yields, in the same spectral interval, of a single transient species (*e.g.* $^{\bullet}OH$) in the various lake water samples, one can see that the values are significantly different but that the differences are typically below (and often much below) an order of magnitude. This means that, when specific data for a given water sample are not available, it is conceivable to model the indirect photochemical processes induced by $^{3}CDOM^{*}$, $^{1}O_2$ and $^{\bullet}OH$ by using average values of the formation quantum yields, measured in different environments.

Implications for photochemical reactivity in water columns

The fact that the quantum yields for the generation of reactive transients by irradiated CDOM decrease with increasing wavelength has potentially important implications for the photochemistry of natural water bodies. Actually, visible light undergoes absorption by water components to a lesser extent than UV radiation and it shows a comparatively higher penetration in the water column. Additionally, UVA penetrates more than UVB. Compared to the incident sunlight spectrum, the light field in the lower depths of water bodies is thus deficient in the UV and most notably in the UVB component (Loiselle et al., 2008; Rose et al., 2009). As a consequence, as far as the modelling of photochemical reactions is concerned, the use of wavelength-dependent quantum yields should give different results compared to constant quantum yield values. This section has the goal of assessing the importance of such a difference.

The occurrence of reactive transients in surface waters (such as $^{3}CDOM^{*}$, $^{1}O_2$ and $^{\bullet}OH$) can be modelled as a function of sunlight irradiance, water chemistry and depth, by use of the software APEX (Aqueous Photochemistry of Environmentally-occurring Xenobiotics) (Bodrato and Vione, 2014). APEX takes into account the absorption of radiation in the water column and gives, among other parameters, column-averaged values of the steady-state concentrations of the transient species (referred to a sunlight irradiance of 22 W m^{-2} in the UV, 290-400 nm). An advantage of APEX is that it can model relatively deep water columns of environmental significance, while experiments are usually

limited to very short irradiation path lengths. Steady-state concentrations are calculated from formation rates and decay/scavenging constants (which, in the case of $^{\bullet}OH$, strongly depend on the water chemistry; Hoigné, 1990; Brezonik and Fulkerson-Brekken, 1998; Al Housari et al., 2010). The transient formation rates are computed based on light-absorption calculations in mixtures and on the formation quantum yields. By suitably modifying the APEX code, it is possible to use constant or wavelength-dependent quantum yields for the generation of ^{3}CDOM*, $^1O_2$ and $^{\bullet}OH$ by CDOM.

For the wavelength-dependent quantum yields, three spectral intervals were identified: UVB (from 290 to 320 nm), UVA (from 321 to 399 nm) and blue, here taken as representative of the range 400-500 nm, above which the absorption of sunlight by CDOM becomes very low (Loiselle et al., 2009). For each transient species and each spectral interval, the formation quantum yields reported in Figure 2 for the different lake water samples were averaged, and the average values were used as input data for the software. The average values are also reported in Table S3 (SM). Note that, in the case of $^1O_2$, a ^{3}CDOM*-induced measurement bias cannot be excluded for the mountain lakes (Balma and SdS) on the basis of the $\Phi_{^1O_2}$ trend. For this reason, the average $\Phi_{^1O_2}$ values were determined using data from the lowland lakes only (Avigliana, Candia and Viverone).

Using the above input data, the steady-state concentrations of ^{3}CDOM*, $^1O_2$ and $^{\bullet}OH$ can be computed as a function of water depth, about which a comment is needed. For a given depth *d*, APEX reports the column-averaged concentration of each transient (under the hypothesis that the water column is well mixed). Such an average takes into account the elevated values (high photoactivity) in the uppermost layer near the surface, as well as the low ones at the bottom (Bodrato and Vione, 2014). Therefore, for the transient *i*, a plot of the steady-state [*i*] *vs. d* is not a depth profile, but rather the comparison between water bodies having different depths.

Based on the above premises, Figure 3 reports the average steady-state concentrations [*i*] of ^{3}CDOM* (3a, 3b), $^1O_2$ (3c, 3d) and of $^{\bullet}OH$ produced by CDOM (3e, 3f), for water columns with different depths (up to 10 m, with 22 W m^{-2} UV irradiance of sunlight at the water surface). The maximum column depth was 10 m, to make the mixing hypothesis reasonable (Wetzel, 2001). The model calculations were carried out in two different scenarios, with DOC values of 1 mg C L^{-1} (3a, 3c, 3e) and of 5 mg C L^{-1} (3b, 3d, 3f). Hereafter, they will be indicated as low-DOC and high-DOC conditions, respectively. Other water parameters of photochemical significance were 1 mM bicarbonate and 10 μM carbonate (note that only $^{\bullet}OH$ produced by CDOM is reported, while the contributions of nitrate and nitrite are not considered here). APEX uses the DOC value to quantify the scavenging rate constant of radical species ($^{\bullet}OH$ in the present case) by DOM and to model the absorption spectrum $A_1(\lambda)$ of surface waters, which is mostly accounted for by CDOM. The calculation of the sunlight photon flux absorbed by CDOM allows the modelling of CDOM photochemistry.

The solid curves of Figure 3 represent the [*i*] values calculated with the formation quantum yields reported in Table S3 and referred to the three different spectral intervals (wavelength-variable quantum

yields, hereafter $\Phi_i(\lambda)$). The dashed curves were obtained with quantum yields that did not vary with wavelength (hereafter, constant Φ_i). The constant Φ_i values were selected so as to obtain, in the shallowest water bodies ($d \rightarrow 0$), the same concentrations [i] as for the $\Phi_i(\lambda)$ approach. To do so, it was used $\Phi_{^3CDOM^*} = 7.7 \cdot 10^{-3}$, $\Phi_{^1O_2} = 5.6 \cdot 10^{-3}$, and $\Phi_{^\bullet OH}^{CDOM} = 8.7 \cdot 10^{-6}$. Figure 3 shows that, in all the cases, the [i] values obtained by using $\Phi_i(\lambda)$ have a faster decrease with depth than those obtained with constant Φ_i. More specifically, in the low-DOC scenario for d = 10 m, [^{3}CDOM*] obtained with $\Phi_i(\lambda)$ is lower by 40% compared to constant Φ_i, while [$^1O_2$] and [$^\bullet$OH] are lower by 30%. In the high-DOC scenario for d = 10 m, the steady-state concentrations obtained with $\Phi_i(\lambda)$ are about one-half of those obtained with constant Φ_i. Therefore, in relatively deep water bodies, the use of wavelength-variable quantum yields has important implications for the assessment of the steady-state [i] values. Because the rates of indirect photochemistry processes are proportional to [i] (Hoigné, 1990), there are implications as well for the modelling of the photochemical fate of pollutants.

Conclusions

- The formation quantum yields of ^{3}CDOM* and $^\bullet$OH by irradiated CDOM had an important decrease with increasing wavelength, from the UVB to the UVA and blue ranges. A possible explanation is that radiation at the longer wavelengths is preferentially absorbed by HMW CDOM, which is less photoactive than LMW CDOM because of radiationless and reactionless phenomena of internal conversion.
- In the three lowland lakes, the formation quantum yields of $^1O_2$ had a less marked decrease with increasing wavelength compared to ^{3}CDOM* or $^\bullet$OH. This issue is unlikely accounted for by a ^{3}CDOM*-related bias on the measurement of $^1O_2$, which would rather produce a $\Phi_{^1O_2}$ trend that is similar to $\Phi_{^3CDOM^*}$. The measured production of $^1O_2$ at the longer wavelengths might be connected with the photochemical properties of HMW CDOM, including for instance the elevated $^1O_2$ levels in hydrophobic CDOM cores, or the formation of less reactive triplet states upon long-wavelength irradiation.
- The formation quantum yields of the transient species in the same spectral interval were different among the studied lakes, but differences were relatively small when taking into account the potentially huge environmental variability (including differences in trophic state and surrounding environment). Indeed, quantum yield values for the studied lake water samples ranged within an order of magnitude or less. This issue suggests that it would be approximate but acceptable to use average quantum yield values to model photochemical processes in natural waters.
- The wavelength trend of the formation quantum yields has a significant impact on the modelling of the steady state concentrations of the transient species, compared to the use of wavelength-

independent quantum yields. The issue becomes more evident with increasing depth, and it is quite marked for d = 10 m. The reason is that the average light field in deep water is considerably different compared to the water surface, due to radiation absorption by CDOM that attenuates the lower wavelengths of UV and visible light more strongly than the higher wavelengths.

Acknowledgements

DV acknowledges financial support from Università di Torino - EU Accelerating Grants, project TO_Call2_2012_0047 (Impact of radiation on the dynamics of dissolved organic matter in aquatic ecosystems - DOMNAMICS).

References

Al Housari, F., Vione, D., Chiron, S., Barbati, S., 2010. Reactive photoinduced species in estuarine waters. Characterization of hydroxyl radical, singlet oxygen and dissolved organic matter triplet state in natural oxidation processes. Photochemical and Photobiological Sciences 9, 78-86.

Anesio, A. M., Graneli, W., 2003. Increased photoreactivity of DOC by acidification: Implications for the carbon cycle in humic lakes. Limnology and Oceanography 48, 735-744.

Anesio, A.M., Graneli, W., 2004. Photochemical mineralization of dissolved organic carbon in lakes of differing pH and humic content. Archiv für Hydrobiologie 160, 105-116.

Bodrato, M., Vione, D., 2014. APEX (Aqueous Photochemistry of Environmentally occurring Xenobiotics): A free software tool to predict the kinetics of photochemical processes in surface waters. Environmental Science: Processes and Impacts 16, 732-740.

Boreen, A.L., Arnold, W.A., McNeill, K., 2003. Photodegradation of pharmaceuticals in the aquatic environment: a review. Aquatic Sciences 65, 320-341.

Bracchini, L., Dattilo, A. M., Falcucci, M., Hull, V., Tognazzi, A., Rossi, C., Loiselle, S. A., 2011. Competition for spectral irradiance between epilimnetic optically active dissolved and suspended matter and phytoplankton in the metalimnion. Consequences for limnology and chemistry. Photochemical and Photobiological Sciences 10, 1000-1013.

Braslavsky, S.E., 2007. Glossary of terms used in photochemistry. third edition. Pure and Applied Chemistry 79, 293-465.

Brezonik, P. L., Fulkerson-Brekken, J., 1998. Nitrate-induced photolysis in natural waters: Controls on concentrations of hydroxyl radical photo-intermediates by natural scavenging agents. Environmental Science and Technology 32, 3004-3010.

Buxton, G.V., Greenstock, C.L., Helman, W.P., Ross, A.B., 1988. Critical review of rate constants for reactions of hydrated electrons, hydrogen atoms and hydroxyl radicals ($^{\bullet}OH/O^{-\bullet}$) in aqueous solution. Journal of Physical and Chemical Reference Data 17, 1027-1284.

Canonica, S., Freiburghaus, M., 2001. Electron-rich phenols for probing the photochemical reactivity of freshwaters. Environmental Science and Technology 35, 690-695.

Canonica, S., Hellrung, B., Mueller, P., Wirz, J., 2006. Aqueous oxidation of phenylurea herbicides by triplet aromatic ketones. Environmental Science and Technology 40, 6636-6641.

Cavani, L., Halladja, S., Ter Halle, A., Guyot, G., Corrado, G., Ciavatta, C., Boulkamh, A., Richard, C., 2009. Relationship between photosensitizing and emission properties of peat humic acid fractions obtained by tangential ultrafiltration. Environmental Science and Technology 43, 4348-4354.

Coble, P. G., 1996. Characterization of marine and terrestrial DOM in seawater using excitation-emission spectroscopy. Marine Chemistry 51, 325-346.

De Laurentiis, E., Minella, M., Maurino, V., Minero, C., Brigante, M., Mailhot, G., Vione, D., 2012. Photochemical production of organic matter triplet states in water samples from mountain lakes, located below or above the tree line. Chemosphere, 88, 1208-1213.

De Laurentiis, E., Minella, M., Sarakha, M., Marrese, A., Minero, C., Mailhot, G., Brigante, M., Vione, D., 2013a. Photochemical processes involving the UV absorber benzophenone-4 (2-hydroxy-4-methoxybenzophenone-5-sulphonic acid) in aqueous solution: Reaction pathways and implications for surface waters. Water Research 47, 5943-5953.

De Laurentiis, E., Buoso, S., Maurino, V., Minero, C., Vione, D., 2013b. Optical and photochemical characterization of chromophoric dissolved organic matter from lakes in Terra Nova Bay, Antarctica. Evidence of considerable photoreactivity in an extreme environment. Environmental Science and Technology 47, 14089-14098.

Del Vecchio, R., Blough, N. V., 2004. On the origin of the optical properties of humic substances. Environmental Science and Technology 38, 3885-3891.

Deister, U., Warneck, P., Wurzinger, C., 1990. OH radicals generated by NO_3^- photolysis in aqueous solution: Competition kinetics and a study of the reaction $\cdot^{\bullet}OH + CH_2(OH)SO_3^-$. Berichte der Bunsengesellschaft für Physikalische Chemie 94, 594-599.

Galbavy, E. S., Ram, K., Anastasio, C., 2010. 2-Nitrobenzaldehyde as a chemical actinometer for solution and ice photochemistry. Journal of Photochemistry and Photobiology A: Chemistry 209, 186-192.

Glover, C. M., Rosario-Ortiz, F. L., 2013. Impact of halides on the photoproduction of reactive intermediates from organic matter. Environmental Science and Technology 47, 13949-13956.

Golanoski, K. S., Fang, S., Del Vecchio, R., Blough, N. V., 2012. Investigating the mechanism of phenol photooxidation by humic substances. Environmental Science and Technology 46, 3912-3920.

Grebel, J. E., Pignatello, J. J., Mitch, W. A., 2011. Sorbic acid as a quantitative probe for the formation, scavenging and steady-state concentrations of the triplet-excited state of organic compounds. Water Research 45, 6535-6544.

Halladja, S., Ter Halle, A., Aguer, J.-P., Boulkamh, A., Richard, C., 2007. Inhibition of humic substances mediated photooxygenation of furfuryl alcohol by 2,4,6-trimethylphenol. Evidence for reactivity of the phenol with humic triplet excited states. Environmental Science and Technology 41, 6066-6073.

Hoigné, J., 1990. Formulation and calibration of environmental reaction kinetics: Oxidations by aueous photooxidants as an example. In Stumm, W. (ed.), Aquatic Chemical Kinetics, Wiley, NY, pp. 43-70.

Iesce, R. M., Cermola, F., Graziano, M. L., Montella, S., Di Gioia, L., Isidori, M., 2004. Sensitized photooxygenation of the fungicide furalaxyl. Environmental Science and Pollution Research 11, 222-226.

Kieber, R.J., Seaton, P.J., 1995. Determination of subnanomolar concentrations of nitrite in natural waters. Analytical Chemistry 67, 3261-3264.

Latch, D. E., McNeill, K., 2006. Microheterogeneity of singlet oxygen distributions in irradiated humic acid solutions. Science 311, 1743-1747.

Lee, E., Glover, C. M., Rosario-Ortiz, F. L., 2013. Photochemical formation of hydroxyl radical from effluent organic matter: Role of composition. Environmental Science and Technology 47, 12073-12080.

Lester, Y., Sharpless, C. M., Mamane, H., Linden, K. G., 2013. Production of photo-oxidants by dissolved organic matter during UV water treatment. Environmental Science and Technology 47, 11726-11733.

Loiselle, S. A., Azza, N., Cozar, A., Bracchini, L., Tognazzi, A., Dattilo, A., Rossi, C., 2008. Variability in factors causing light attenuation in Lake Victoria. Freshwater Biology 53, 535-545.

Loiselle, S. A., Bracchini, L., Dattilo, A. M., Ricci, M., Tognazzi, A., Cozar, A., Rossi, C., 2009. Optical characterization of chromophoric dissolved organic matter using wavelength distribution of absorption spectral slopes. Limnology and Oceanography 54, 590-597.

Maddigapu, P. R., Bedini, A., Minero, C., Maurino, V., Vione, D., Brigante, M., Mailhot, G., Sarakha, M., 2010. The pH-dependent photochemistry of anthraquinone-2-sulfonate. Photochemical and Photobiological Sciences 9, 323-330.

Méndez-Díaz, J. D., Shimabuku, K. K., Ma, J., Enumah, Z. O., Pignatello, J. J., Mitch, W. A., Dodd, M. C., 2014. Sunlight-driven photochemical halogenation of dissolved organic matter in

seawater: A natural abiotic source of organobromine and organoiodine. Environmental Science and Technology 48, 7418-7427.

Minella, M., Merlo, M. P., Maurino, V., Minero, C., Vione, D., 2013. Transformation of 2,4,6-trimethylphenol and furfuryl alcohol, photosensitised by Aldrich humic acids subject to different filtration procedures. Chemosphere 90, 306-311.

Mopper, K., Zhou, X., 1990. Hydroxyl radical photoproduction in the sea and its potential impact on marine processes. Science 250, 661-664.

Mostafa, S., Rosario-Ortiz, F. L., 2013. Singlet oxygen formation from wastewater organic matter. Environmental Science and Technology 47, 8179-8186.

Mostafa, S., Korak, J. A., Shimabuku, K., Glover, C. M., Rosario-Ortiz, F. L., 2014. Relation between optical properties and formation of reactive intermediates from different size fractions of organic matter. In: Advances in the Physicochemical Characterization of dissolved Organic Matter: Impact on Natural and Engineered Systems. Rosario-Ortiz, F. L. (ed.), ACS Symposium Series, Vol. 1160, pp. 159-179.

Page, S.E., Arnold, W.A., McNeill, K., 2011. Assessing the contribution of free hydroxyl radical in organic matter-sensitized photohydroxylation reactions. Environmental Science and Technology 45, 2818-2825.

Peuravuori, J., Pihlaja, K., 1997. Molecular size distribution and spectroscopic properties of aquatic humic substances. Analytica Chimica Acta 337, 133-149.

Piccini, C., Conde, D., Pernthaler, J., Sommaruga, R., 2013. Photoalteration of macrophyte-derived chromophoric dissolved organic matter induces growth of single bacterial populations in a coastal lagoon. Journal of Limnology 72, 582-591.

Ruiz-Gonzales, C., Simo, R., Sommaruga, R., Gasol, J. M., 2013. Away from darkness: a review on the effects of solar radiation on heterotrophic bacterioplankton activity. Frontiers in Microbiology 4, 131.

Rodgers, M. A. J., Snowden, P. T., 1982. Lifetime of $^1O_2$ in liquid water as determined by time-resolved infrared luminescence measurements. Journal of the American Chemical Society 104, 5541-5543.

Rose, K. C., Williamson, C. E., Saros, J. E., Sommaruga, R., Fischer, J. M., 2009. Differences in UV transparency and thermal structure between alpine and subalpine lakes: implications for organisms. Photochemical and Photobiological Sciences 8, 1244-1256.

Ruggeri, G., Ghigo, G., Maurino, V., Minero, C., Vione, D., 2013. Photochemical transformation of ibuprofen into harmful 4-isobutylacetophenone: Pathways, kinetics, and significance for surface waters. Water Research 47, 6109-6121.

Sharpless, C. M., 2012. Lifetimes of triplet dissolved natural organic matter (DOM) and the effect of $NaBH_4$ reduction on singlet oxygen quantum yields: Implications for DOM photophysics. Environmental Science and Technology 46, 3912−3920.

Sharpless, C. M., Blough, N. V., 2014. The importance of charge-transfer interactions in determining chromophoric dissolved organic matter (CDOM) optical and photochemical properties. Environmental Science: Processes and Impacts 16, 654-671.

Sulzberger, B., Durisch-Kaiser, E., 2009. Chemical characterization of dissolved organic matter (DOM): A prerequisite for understanding UV-induced changes of DOM absorption properties and bioavailability. Aquatic Sciences 71, 104-126.

Sur, B., Rolle, M., Minero, C., Maurino, V., Vione, D., Brigante, M., Mailhot, G., 2011. Formation of hydroxyl radicals by irradiated 1-nitronaphthalene (1NN): Oxidation of hydroxyl ions and water by the 1NN triplet state. Photochemical and Photobiological Sciences 10, 1817-1824.

Trubetskoj, O.A., Trubetskaya, O.E., Richard, C., 2009. Photochemical activity and fluorescence of electrophoretic fractions of aquatic humic matter. Water Research 36, 518-524.

Vahatalo, A. V., Salonen, K., Munster, U., Jarvinen, M., Wetzel, R. G., 2003. Photochemical transformation of allochthonous organic matter provides bioavailable nutrients in a humic lake. Archiv für Hydrobiologie 156, 287-314.

Vahatalo, A. V., Wetzel, R. G., 2008. Long-term photochemical and microbial decomposition of wetland-derived dissolved organic matter with alteration of C-13:C-12 mass ratio. Limnology and Oceanography 53, 1387-1392.

Vione, D., Lauri, V. Minero, C., Maurino, V., Malandrino, M., Carlotti, M. E., Olariu, R. I., Arsene, C., 2009. Photostability and photolability of dissolved organic matter upon irradiation of natural water samples under simulated sunlight. Aquatic Sciences 71, 34-45.

Vione, D., Minella, M., Maurino, V., Minero, C., 2014. Indirect photochemistry in sunlit surface waters: Photoinduced production of reactive transient species. Chemistry: A European Journal 20, 10590-10606.

Wetzel, R. G., 2001. Limnology: Lake and River Ecosystems. 3rd edition, Academic Press.

Wilkinson, F., Brummer, J., 1981. Rate constants for the decay and reactions of the lowest electronically excited singlet-state of molecular oxygen in solution. Journal of Physical and Chemical Reference Data 10, 809-1000.

White, E. M., Vaughan, P. P., Zepp, R. G., 2003. Role of the photo-Fenton reaction in the production of hydroxyl radicals and photobleaching of colored dissolved organic matter in a coastal river of the southeastern United States. Aquatic Sciences 65, 402-414.

Xiao, Y. H., Sara-Aho, T., Hartikainen, H., Vahatalo, A V., 2013. Contribution of ferric iron to light absorption by chromophoric dissolved organic matter. Limnology and Oceanography 58, 653-662.

Zhang, Y. L., Liu, X. H., Osburn, C. L., Wang, M. Z., Qin, B. Q., Zhou, Y. Q., 2013. Photobleaching response of different sources of chromophoric dissolved organic matter exposed to natural solar radiation using absorption and excitation-emission matrix spectra. Plos One 8, e77515.

Table 1. Chemical and spectroscopic parameters of the studied lake water samples. Error bounds are reported as ±1 standard deviation (±σ) of multiple analyses (at least 2). Note that TON (total organic nitrogen) is calculated from total nitrogen (TN) as follows: TON = TN – (NO_3^- + NO_2^- + NH_4^+), after conversion of the values of the inorganic N species from µg L^{-1} to mg L^{-1}. The DL (detection limit) was around 0.02 mg L^{-1} for Na^+, K^+ and NH_4^+ and around 0.01 mg L^{-1} for Cl^- and NO_3^-. Total dissolved Fe (determined by inductively coupled plasma, see SM) in the filtered lake water samples was in all cases below 2.5 µg L^{-1}.

Lake	**Na^+, mg L^{-1}**	**K^+, mg L^{-1}**	**Mg^{2+}, mg L^{-1}**	**Ca^{2+}, mg L^{-1}**	**NH_4^+, µgN L^{-1}**	**Cl^-, mg L^{-1}**	**SO_4^{2-}, mg L^{-1}**	**NO_3^-, µgN L^{-1}**
Avigliana	4.44±0.39	2.30±0.39	28.1±1.2	30.3±2.1	< DL	7.51±0.66	24.4±2.4	1.11±0.05
Candia	1.44±0.51	< DL	6.6±0.5	18.2±1.1	0.26±0.06	4.53±0.69	3.72±0.26	< DL
Viverone	6.62±0.41	5.30±0.36	33.3±1.5	55.9±4.2	0.60±0.06	4.77±0.69	17.5±1.7	< DL
Balma	< DL	< DL	0.71±0.36	1.34±0.45	0.34±0.06	< DL	1.04±0.19	0.20±0.01
SdS (*)	< DL	< DL	1.01±0.63	7.63±0.40	0.36±0.06	< DL	3.36±0.23	1.02±0.05

Lake	**NO_2^-, µgN L^{-1}**	**DOC, mgC L^{-1}**	**IC, mgC L^{-1}**	**pH**	**TN, mgN L^{-1}**	**TON, mgN L^{-1}**	**E_2/E_3**	**S, µm^{-1}**
Avigliana	0.055±0.004	5.81±1.51	32.0±0.4	8.1	0.78±0.11	0.55±0.12	11.1	21.8±0.7
Candia	0.003±0.001	6.90±1.01	11.8±0.4	7.7	0.69±0.11	0.64±0.12	9.2	19.7±0.7
Viverone	0.001	5.52±1.32	21.1±0.4	7.9	0.70±0.10	0.58±0.11	11.3	20.7±1.0
Balma	0.008±0.001	3.25±0.14	0.68±0.01	6.4	0.35±0.09	0.24±0.10	5.5	15.1±0.3
SdS (*)	0.005±0.003	0.59±0.06	1.67±0.01	6.9	0.34±0.09	0.07±0.11	4.6	13.7±1.2

(*) Short for “Sottano della Sella”.

Table 2. Transformation rates of TMP and FFA, and formation rates of phenol, ^{3}CDOM*, $^1O_2$ and $^\bullet$OH. The rates of TMP, FFA and phenol were experimentally measured, those of ^{3}CDOM*, $^1O_2$ and $^\bullet$OH were calculated based on equations (9), (10) and (11), respectively. The formation rate of $^\bullet$OH is referred to the contribution of irradiated CDOM, after subtracting for the $^\bullet$OH formation rate by nitrate and nitrite. The error bounds represent the sigma-level variability of replicated runs (±σ). In some cases, when required by the significant figures and for table readability issues, errors have been approximated in excess to "0.1" or "0.01".

		Avigliana	**Candia**	**Viverone**	**Balma**	**SdS**
R_{TMP}, 10^{-9} M s^{-1}	***UVB***	18.4±0.1	19.5±0.1	14.4±0.1	11.9±0.1	13.0±0.1
	UVA	13.3±0.2	10.5±0.2	8.43±0.19	4.54±0.03	3.36±0.02
	Blue	2.14±0.04	2.46±0.08	1.36±0.04	1.17±0.01	0.61±0.01
R_{FFA}, 10^{-10} M s^{-1}	***UVB***	3.82±0.03	3.60±0.03	2.95±0.01	4.69±0.03	2.28±0.01
	UVA	3.32±0.03	2.88±0.04	2.42±0.02	1.99±0.02	1.03±0.09
	Blue	1.36±0.02	1.51±0.05	0.70±0.02	0.93±0.03	Neglig.(*)
R_{Phenol}, 10^{-11} M s^{-1}	***UVB***	1.72±0.09	1.55±0.03	1.19±0.09	1.47±0.12	0.48±0.07
	UVA	1.43±0.07	0.84±0.04	0.20±0.01	0.93±0.06	0.23±0.02
	Blue	0.36±0.01	0.13±0.01	0.33±0.01	0.32±0.04	0.08±0.01
$R_{^3CDOM^*}$, 10^{-9} M s^{-1}	***UVB***	15.0±0.1	16.3±0.1	10.3±0.1	7.38±0.32	8.65±0.73
	UVA	13.4±0.2	10.2±0.2	7.78±0.22	3.23±0.03	1.85±0.02
	Blue	2.04±0.05	2.42±0.09	1.14±0.04	0.91±0.01	0.26±0.01
$R_{^1O_2}$, 10^{-9} M s^{-1}	***UVB***	5.12±0.08	4.65±0.05	3.23±0.02	7.03±0.06	1.77±0.01
	UVA	6.82±0.06	5.86±0.11	4.85±0.02	3.90±0.04	1.82±0.27
	Blue	2.98±0.04	3.30±0.09	1.52±0.03	2.02±0.06	Neglig.(*)
$R_{^\bullet OH}^{CDOM}$, 10^{-11} M s^{-1}	***UVB***	1.80±0.09	1.63±0.04	1.25±0.09	1.54±0.12	0.50±0.08
	UVA	1.50±0.08	0.88±0.04	0.20±0.01	0.97±0.07	0.23±0.02
	Blue	0.38±0.05	0.14±0.01	0.35±0.01	0.33±0.01	0.08±0.01

(*) The experimental rate was not significantly different from that observed in Milli-Q water.

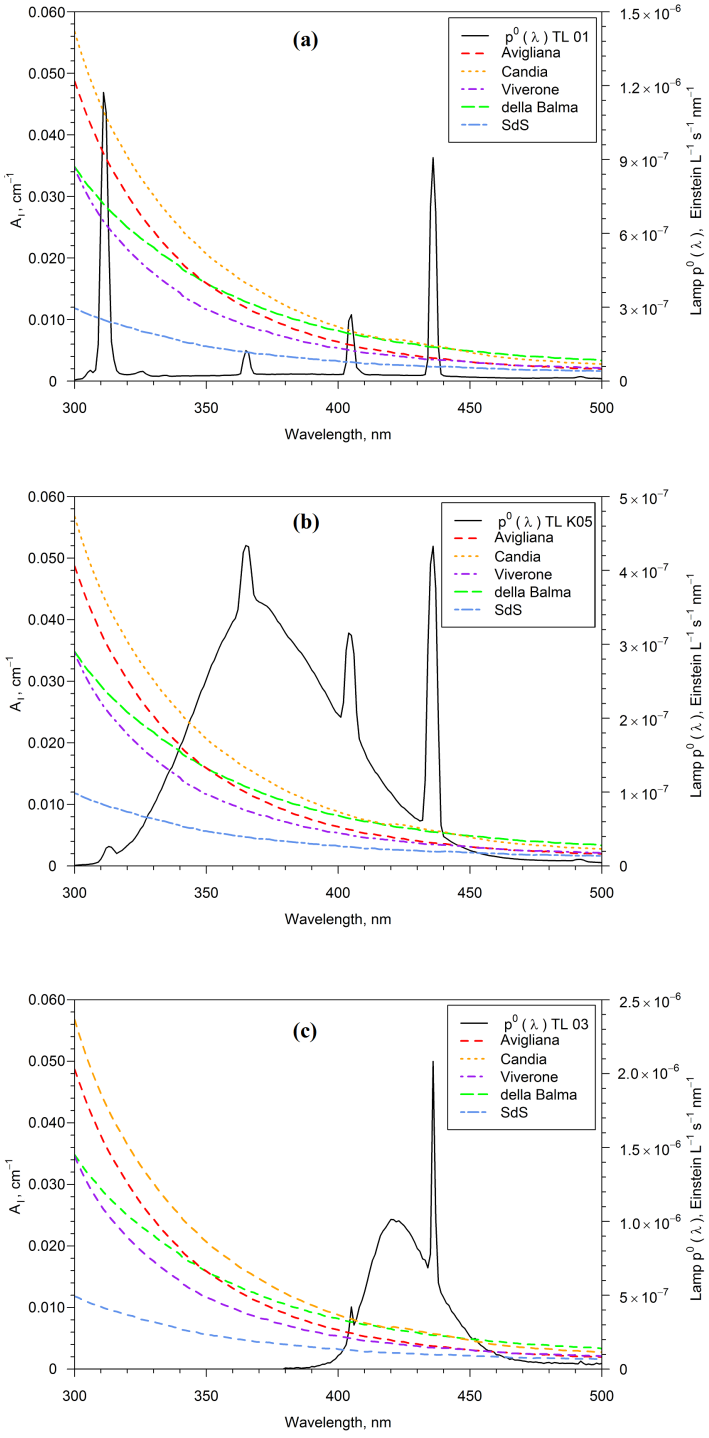

Figure 1. Absorption spectra ($A_1(\lambda)$) of the studied lake water samples. Emission spectra ($p°(\lambda)$) of the used lamps: **(a)** UVB (Philips TL 01); **(b)** UVA (Philips TLK 05); **(c)** blue (Philips TLK 03).

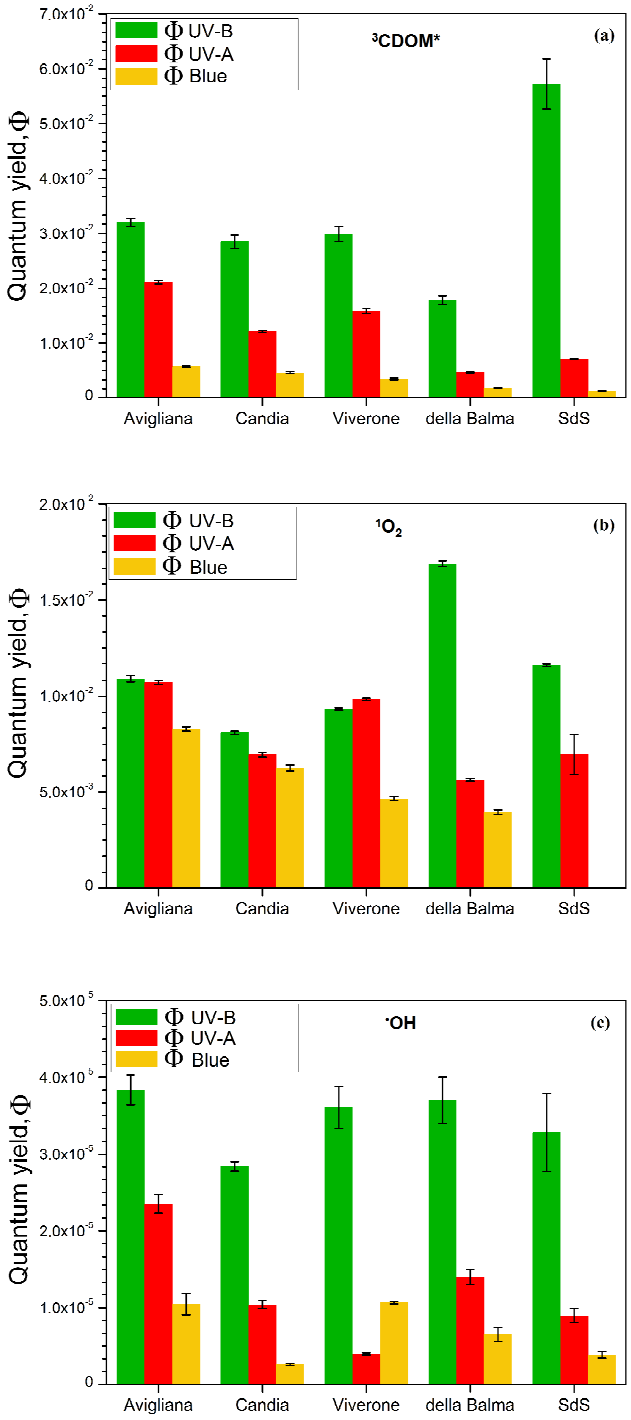

Figure 2. Formation quantum yields of the reactive transients upon irradiation of the studied lake water samples in the different spectral intervals (UVB, UVA and blue): **(a)** $\Phi_{^3CDOM*}$; **(b)** $\Phi_{^1O_2}$; **(c)** $\Phi_{\cdot OH}^{CDOM}$.

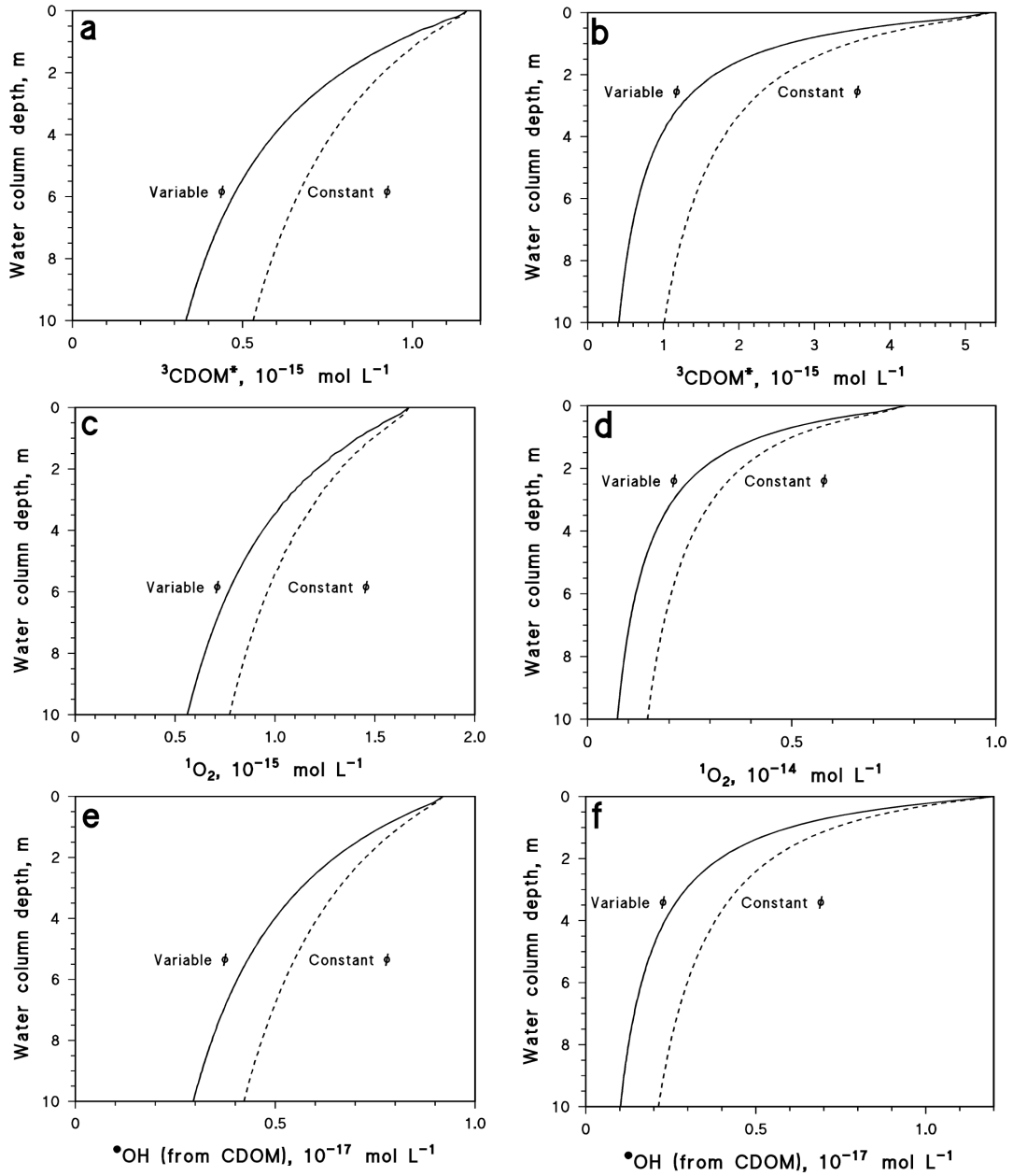

Figure 3. Column-averaged steady-state concentrations of the studied transient species (X-axis) for different values of the water column depth (Y-axis). The solid curves represent the results of calculations carried out with formation quantum yields ($\Phi_{^3CDOM*}$, $\Phi_{^1O_2}$ and $\Phi_{^\bullet OH}^{CDOM}$) that varied depending on the considered wavelength interval (UVB, UVA or blue, see Table S3). The dashed curves represent calculation results with wavelength-independent quantum yields, chosen to match the steady-state concentrations of the solid curves for $d \to 0$.
(a) ^{3}CDOM*, DOC = 1 mg C L^{-1}; **(b)** ^{3}CDOM*, DOC = 5 mg C L^{-1}; **(c)** $^1O_2$, DOC = 1 mg C L^{-1}; **(d)** $^1O_2$, DOC = 5 mg C L^{-1}; **(e)** $^\bullet$OH, DOC = 1 mg C L^{-1}; **(f)** $^\bullet$OH, DOC = 5 mg C L^{-1}. Other water conditions: 1 mM bicarbonate, 10 µM carbonate, 22 W m^{-2} UV irradiance of sunlight. Note that the reported steady-state [$^\bullet$OH] is referred to the photochemistry of CDOM alone and does not take into account the contributions to $^\bullet$OH formation by the photolysis of nitrate and nitrite.